frontiers | Frontiers in Neuroscience RETRACTED ON 27 NOVEMBER 2025

TYPE Original Research
PUBLISHED 16 December 2024
DOI 10.3389/fnins.2024.1491343

OPEN ACCESS

EDITED BY
Marcos Roberto De Oliveira,
Federal University of Rio Grande do Sul, Brazil

REVIEWED BY
Li Zhang,
Nanjing University, China
Yuxing Zhang,
University of Texas Health Science Center at Houston, United States

*CORRESPONDENCE
Fang Liu
✉ 2289797960@qq.com
Hua Hu
✉ hh201201201@163.com
Chun Guo
✉ chunguosm@163.com

†These authors have contributed equally to this work

RECEIVED 04 September 2024
ACCEPTED 03 December 2024
PUBLISHED 16 December 2024
RETRACTED 27 November 2025

CITATION
Wang X, Lin X, Chen Z, Long H, Zhou X, Lei S, Liu J, Dong H, Liu F, Hu H and Guo C (2024) Annao Pingchong decoction attenuates oxidative stress and neuronal apoptosis following intracerebral hemorrhage via RAGE-NOX2/4 axis.
Front. Neurosci. 18:1491343.
doi: 10.3389/fnins.2024.1491343

RETRACTED: Annao Pingchong decoction attenuates oxidative stress and neuronal apoptosis following intracerebral hemorrhage via RAGE-NOX2/4 axis

Xu Wang[1,2†], Xiaoyuan Lin[1†], Zilin Chen[3], Hongping Long[1], Xuqing Zhou[1], Shihui Lei[1], Jian Liu[1], Huan Dong[1], Fang Liu[1*], Hua Hu[2*] and Chun Guo[1*]

[1]Experiment Center of Medical Innovation, The First Hospital of Hunan University of Chinese Medicine, Changsha, China, [2]Department of Neurology, The First Hospital of Hunan University of Chinese Medicine, Changsha, China, [3]Department of Pediatrics, Guanganmen Hospital, China Academy of Traditional Chinese Medicine, Beijing, China

Background: Intracerebral hemorrhage (ICH) is a severe condition associated with high mortality and disability rates. Oxidative stress plays a critical role in the development of secondary brain injury (SBI) following ICH. Previous research has demonstrated that Annao Pingchong decoction (ANPCD) treatment for ICH has antioxidant effects, but the exact mechanism is not yet fully understood.

Objective: This study aimed to investigate the neuroprotective effects of ANPCD on oxidative stress and neuronal apoptosis after ICH by targeting the receptor for advanced glycation end products (RAGE)-NADPH oxidase (NOX) 2/4 signaling axis.

Methods: The research involved the creation of rat ICH models, the mNSS assay to assess neurological function, Nissl staining to evaluate neuronal damage, and biochemical assays to measure oxidative and antioxidant levels. The expression of RAGE-NOX2/4 axis proteins was analyzed using western blotting and immunofluorescence, while neuronal apoptosis was assessed with TUNEL staining. Furthermore, after performing quality control of drug-containing serum using UPLC-MS/MS, we employed an *in vitro* model of heme-induced injury in rat cortical neurons to investigate the neuroprotective mechanisms of ANPCD utilizing RAGE inhibitors.

Results: The findings indicated that ANPCD improved neurological deficits, reduced neuronal damage, decreased ROS and MDA levels, and increased the activities enzymatic activities of SOD, CAT, GSH and GPX. Additionally, it suppressed the RAGE-NOX2/4 signaling axis and neuronal apoptosis.

Conclusion: ANPCD exhibits neuroprotective effects by inhibiting the RAGE-NOX2/4 signaling axis, thereby alleviating neuronal oxidative stress and apoptosis following ICH.

KEYWORDS

Annao Pingchong decoction, intracerebral hemorrhage, NOX2/4, RAGE, oxidative stress

1 Introduction

Intracerebral hemorrhage (ICH) refers to the non-traumatic rupture and subsequent bleeding of blood vessels within the brain parenchyma, typically presenting with an acute onset and severe clinical conditions. The one-year mortality rate can reach up to 59%, and more than 80% of survivors experience permanent disability (Ren et al., 2020). Surgical intervention is the principal treatment modality for ICH; however, the non-regenerative nature of neurons poses a substantial challenge to the restoration of neurological function in affected individuals. Post-hemorrhagic brain injury includes primary brain injury caused by the space-occupying effects of a hematoma. It also involves secondary brain injury (SBI) resulting from pathological responses to hemorrhagic lesions. Oxidative stress and inflammation are critical pathological mechanisms contributing to SBI. There is a growing recognition among researchers of the necessity to prevent the progression of SBI following ICH in order to enhance the recovery of neurological function in patients with ICH (Bautista et al., 2021).

Following ICH, the lysis of red blood cells can result in the production of cytotoxic substances that induce oxidative stress in neurons and trigger neuroimmune responses, which in turn lead to additional oxidative damage to cells (Rendevski et al., 2023). Excessive reactive oxygen species (ROS) can directly cause lipid peroxidation and DNA damage in neurons, compromising their structural integrity and promoting apoptosis (Shadfar et al., 2023). Furthermore, these ROS can exacerbate neuroinflammation and disrupt the blood–brain barrier, ultimately contributing to neuronal death (Ding et al., 2022). The process of cell damage induced by ROS is not transient. Oxidative stress progressively intensifies and disseminates to surrounding tissues, resulting in additional neuronal damage and exacerbation of neurological deficits. Furthermore, this phenomenon is interconnected with inflammation, another critical mechanism of SBI, which both induces and exacerbates oxidative stress, collectively contributing to nerve damage (Wu et al., 2022). Therefore, it is crucial to intervene with pharmacological agents during the early stages of ICH to mitigate the initial processes of neuronal oxidative stress and inflammation, thereby safeguarding patients' neurological function. Nonetheless, no effective clinical drugs have yet been identified to prevent the onset and progression of SBI (Chen et al., 2021).

The receptor for advanced glycation end products (RAGE) is a transmembrane receptor present in various cell types, including neurons, capable of binding to endogenous extracellular ligands and intracellular effectors such as heme, S100B, and HMGB1 (Yepuri et al., 2021). Research indicates that RAGE levels in tissues and apoptotic cells surrounding hematomas significantly increase following ICH, accompanied by heightened inflammatory responses and oxidative stress (Piras et al., 2016; Ray et al., 2016). While considerable attention has been directed toward the association between RAGE and tissue inflammation, the cellular damage resulting from oxidative stress due to RAGE activation is also of paramount importance. NADPH oxidase (NOX) is a membrane-bound enzyme complex that produces ROS and is primarily located in the cell membrane, with subtypes NOX2 and NOX4 found in neurons (Terzi and Suter, 2020; Ding et al., 2023). Increased NOX activity results in excessive ROS accumulation and subsequent cellular oxidative damage. Studies have demonstrated that the inhibition of RAGE receptor activation and NOX activity can mitigate brain tissue damage and neurological deficits in rat models of ICH (Yang et al., 2015; Xie et al., 2020). Overactive RAGE can enhance NOX activity, leading to the generation of elevated levels of ROS and causing intracellular oxidation, ultimately resulting in neuronal injury. This interaction between RAGE and NOX may play a critical role in the early oxidative stress observed in ICH. It suggests that the RAGE-NOX signaling axis is vital in mediating neuronal oxidative stress during the initial stages of ICH.

Traditional Chinese medicine, exemplified by Annao Pingchong decoction (ANPCD), has demonstrated therapeutic effects during both the acute and recovery stages of ICH (Guo et al., 2023). Previous research has identified 93 compounds within ANPCD that may offer antioxidant and neuroprotective benefits against various central nervous system diseases. Additionally, studies have indicated that ANPCD exhibits anti-inflammatory, antioxidant, and anti-apoptotic effects in rat models of ICH (Guo et al., 2023; Zhou et al., 2024). However, the specific antioxidant mechanisms underlying ANPCD's effects remain to be fully elucidated. This study employed a rat ICH model and *in vitro* primary neuron cultures to investigate the influence of ANPCD on the RAGE-NOX2/4 signaling axis, as well as its capacity to mitigate oxidative stress and neuronal apoptosis following ICH, thereby highlighting potential therapeutic benefits for neurological deficits.

2 Materials and methods

2.1 Drug preparation

The herbs used in this study were sourced from the Pharmacy Department of the First Hospital of Hunan University of Chinese Medicine in Changsha, Hunan Province, China. The components of ANPCD were shown in Supplementary Table S1, and its preparation was conducted as our previous study mentioned (Guo et al., 2023). Edaravone and Dexborneol (ED) concentrated solution for injection, which are clinical drugs used to alleviate oxidative stress damage in cerebral infarction, were purchased from Simcere Pharmaceutical Co. Ltd. in Nanjing, China.

2.2 ANPCD-medicated serum preparation

SD rats weighing roughly 300 g were given a three-fold dose of ANPCD solution intragastrically for 5 days in a row. One hour after the final dose, blood was taken from the abdominal aorta, and ANPCD-medicated serum was isolated. Blank serum was obtained from the SD rats and given the same volume of physiological saline, and serum was collected in the same manner. The serum was then inactivated by heating it in a 56°C water bath for 30 min, filtered through a 0.22 μm filter membrane, and aliquoted and stored in a −20°C refrigerator for later use.

Abbreviations: ICH, Intracerebral hemorrhage; SBI, secondary brain injury; ANPCD, Annao Pingchong decoction; RAGE, receptor for advanced glycation end products; NOX, NADPH oxidase; mNSS, Modified Neurological Severity Score; ROS, reactive oxygen species; MDA, Malondialdehyde; SOD, superoxide dismutase; CAT, catalase; GSH, glutathione; GPX, glutathione peroxidases; ED, Edaravone and Dexborneol; Bcl-2, B-cell lymphoma 2; Bax, Bcl-2 associated X protein; CytoC, Cytochrome C; MAP2, microtubule-associated protein 2.

2.3 Characterization of QJHGD by ultra performance liquid chromatography–tandem mass spectrometry (UPLC-MS/MS)

A UPLC-MS/MS method was established for the analysis of serum samples. The molecular feature extraction (MFE) function in the Agilent MassHunter Qualitative Analysis Workstation was used. It extracted molecular features from the raw mass spectral data of both blank serum and ANPCD-medicated serum. Subsequently, the Agilent Mass Profile software was utilized to compare the data from the blank serum and the ANPCD-medicated serum, removal of endogenous components from blank sera. Then, characteristic ions related to the *in vivo* components of ANPCD, including mass number, retention time, and abundance, were extracted and analyzed. Blood concentrations were determined using controls for Geniposide (110749–201,919, National Institutes for Food and Drug Control), Baicalin (FX-10139, Chengdu Pufei De Biotech Co., Ltd), and Wogonoside (JOT-10318, Chengdu Pufei De Biotech Co., Ltd).

2.4 Animal grouping and drug administration

Male Sprague–Dawley (SD) rats were sourced from Hunan Slac Jingda Laboratory Animal Co., Ltd., Changsha, China (license No. SCXK (Xiang) 2019–0004). The rats were maintained under standardized conditions, with a temperature of 24 ± 2°C, relative humidity of 50–70%, and a 12-h light–dark cycle. They had *ad libitum* access to food and water. After a one-week acclimatization period, rats weighing between 280 and 320 g were randomly assigned to one of four groups: sham group, ICH model group, ANPCD treatment group (7.5 g/kg, gavage), and ED treatment group (5.4 mg/kg, intraperitoneal injection). Following the exclusion of rats with unsuccessful modeling and those exhibiting excessively low Neurological Deficit Scores, a total of 36 rats, with 9 rats in each group, were included in this experiment. The sham group and ICH model group received saline gavage, the ANPCD group was administered ANPCD via gavage, and the ED group received an intraperitoneal injection of ED. The first dose of treatment was administered within 2 h of ICH induction, followed by daily gavage or intraperitoneal injection. The study protocol received approval from the Ethics Committee for Experimental Animals of the First Hospital of Hunan University of Chinese Medicine (Approval No.: ZYFY20231101-98).

2.5 ICH model

In a previous study (Guo et al., 2023), rats were subjected to an experimental procedure involving cardiac puncture to obtain 50 μL of blood, which was then injected into the left side of the caudate nucleus of the brain. The injection was carefully administered with a constant velocity, targeting a specific location positioned 3 mm laterally to the midline, 1 mm posterior to the bregma, and 6 mm below the skull's surface. Following a 10-min injection period, the needle was partially retracted by approximately 2 mm and left in place for an additional 4 min before being completely removed. The incision site was then sutured and disinfected, and the rats were individually housed for recovery. The sham group underwent an identical procedure, with the exception of the autologous blood injection.

2.6 Neurological deficit score

To assess neurological deficits in rats, we utilized the Modified Neurological Severity Score (mNSS) to evaluate various aspects such as motor function, sensory function, beam balance, reflexes, and abnormal movements. The assessments were conducted at 6, 24, and 72 h after the induction of ICH in rats. The mNSS scores ranged from 0 to 18, with higher scores indicating more severe neurological deficits. Rats with mNSS scores greater than 8 were included in the experiment. Details of the behavioral testing are shown in Supplementary Table S2.

2.7 Primary neuron culture

Primary cortical neurons were prepared from rat embryos of embryonic day 18. Cerebral cortices were collected and dissociated in a mixture of trypsin and collagenase for 10 min. After termination with FBS, cells were centrifuged and plated with DMED/F12 containing 10% FBS (A5670701, Gibco), 1% B27 (17,504,044, Gibco), and 1% penicillin/streptomycin (15,140,122, Gibco). After the cells were cultured at 37°C for at least 4 h, the medium was replaced with Neurobasal (21,103,049, Gibco) containing B27, penicillin/streptomycin, and Glutamax (35,050,061, Gibco). On the 5th day, the medium was changed and the *in vitro* neurons were grouped: normal group (Control), heme group (Heme, 30 μM), blank serum group (Blank serum, 10%), model group (model, 30 μM heme and 10% blank serum), ANPCD-medicated serum group (ANPCD, 30 μM heme and 10% ANPCD-medicated serum), and RAGE inhibitor group (FPS-ZM1, 30 μM heme、10% blank serum and 500 nM FPS-ZM1). The RAGE inhibitor group required intervention with FPS-ZM1 2 h in advance, while the remaining groups were treated with their respective interventions. Subsequent to the administration of the pharmaceutical agents, the subjects were subjected to a series of follow-up tests 1 day later.

2.8 Cell viability detection

In accordance with the instructions provided in the CCK-8 assay kit (CA1210, Solarbio), the CCK-8 stock solution was diluted 10-fold with DMEM/F12 medium to prepare the CCK-8 assay solution. Subsequently, 100 μL of CCK-8 assay solution was added to each well of all groups in 96-well plates, with a blank well also prepared containing only CCK-8 assay solution for comparison. After incubation for 2 h at 37°C, the optical density (OD value) was measured using the multifunctional microplate reader (Enspire, PerkinElmer, USA) at 450 nm. Cell viability was calculated as follows: Cell survival rate (%) = (OD value of experimental group - OD value of blank well) / (OD value of normal group - OD value of blank well) × 100%.

2.9 ROS and mitochondria detection

Neuronal cells were cleaned and incubated with H2DCFDA (50 μM, HY-D0940, MCE) or MitoTracker Red CMXRos (500 nM,

M9940, Solarbio) for 30 min at 37°C, shielded from light. The former was followed by Hoechst (100 μg/mL, C1022, Beyotime) for 15 min under similar conditions. The latter was then fixed with paraformaldehyde and stained with immunofluorescence. The cells were then washed and observed using a laser confocal microscope, with images taken.

2.10 Nissl and TUNEL staining

Brain tissues were fixed in 4% formaldehyde for 3 days and subsequently dehydrated using an automatic tissue dryer (STP-120, Thermo Fisher, UK). The tissues were then embedded in paraffin, and 5 μm thick coronal sections were obtained using a microtome (HM 325, Thermo Fisher, China). Cell samples were fixed with cell fixation solution (E-IR-R114, Elabscience) for 30 min. After dewaxing and rehydration, the sections were stained with a Nissl (G1434, Solarbio) and TUNEL staining kit (A112, Vazyme) following the manufacturer's instructions. The fixed cells only need to be stained with TUNEL staining kit. Images were captured using a light microscope (BX43; Olympus) and laser confocal microscope (LSM800, Zeiss, Germany).

2.11 Measurements of SOD, CAT, GSH, GPX activity, and MDA content

The brain tissues or neuronal cells were homogenised in an ice bath by adding the extracts provided in the kit. Following this, the supernatant was extracted after centrifugation. The experiments were performed according to the instructions provided in the following kits: SOD (BC0175, Solarbio), CAT (BC0205, Solarbio), GSH (BC1175, Solarbio), GPX (BC1195, Solarbio), and MDA (BC0025, Solarbio). The data results were collected using the multifunctional microplate reader.

2.12 Western blotting

Brain tissue and neuronal cells were disrupted with RIPA lysis buffer (AR0105-100, Boster) at an ice bath for 2 h. The samples were then spun at 12,000 r/min for 10 min, and the supernatant collected. Protein concentrations were assessed using a bicinchoninic acid (BCA) protein assay kit (BL521A, Biosharp). Equal protein samples (40 μg) were separated by 10% sodium dodecyl sulfate-polyacrylamide gel electrophoresis (SDS-PAGE) (CW0022S, CWBIO) and transferred to PVDF membranes (IPVH0005, Millipore). The membranes were blocked with 5% skim milk for 30 min at room temperature and incubated overnight at 4°C with NOX2 (1:5000, 19,013-1-AP, Proteintech)、NOX4 (1:1,000, 14,347-1-AP, Proteintech), RAGE (1:1,000, ab216329, Abcam), Bax (1:5,000, ab32503, Abcam), Bcl-2 (1:2,000, ab182858, Abcam), CytoC (1:5,000, 10,993-1-AP, Proteintech) and β-actin (1:10,000, YM3028, ImmunoWay) antibodies. After three 5-min TBST washes, the membranes were incubated with HRP-conjugated secondary antibody (1:5,000) for 1 h at room temperature. Following three additional 5-min TBST washes, protein bands were visualized using enhanced chemiluminescence (ECL) (BL520A, Biosharp) with a high-sensitivity chemiluminescence imaging system (FluorChem R, Bio-Rad Laboratories). Relative protein quantities were determined using ImageJ software.

2.13 Immunofluorescence assay

The brain tissue samples were prepared for antigen retrieval by sectioning them at a thickness of 10 micrometers and mounting them on slides. The sections were then blocked for 1 h using 5% bovine serum albumin, after which they were incubated overnight at 4°C with the following antibodies: NOX2 (1:5,000), NOX4 (1:1,000), and RAGE (1:1,000). Following washing, the sections were incubated for 30 min at 37°C with Goat Anti-Rabbit Antibody (SA00003-2, Proteintech), washed again, and air-dried. To prevent background fluorescence, the sections were then blocked using a DAPI-containing anti-fluorescent attenuating blocker (S2110, Solarbio) and examined under a laser confocal microscope.

The cell samples were fixed with cell fixative for 30 min, and then permeabilized with 0.25% Triton-100X (T8200, Solarbio) to allow for antibody penetration. The cells were subsequently blocked with 5% bovine serum albumin for 30 min and incubated with MAP2 (1:1,000, Proteintech) and the same primary and secondary antibodies described above. The cells were then incubated with the same primary and secondary antibodies described above, followed by DAPI staining for 20 min at room temperature. The samples were then photographed under laser confocal microscope observation.

2.14 Statistical analysis

Statistical analyses were conducted using GraphPad Prism (version 9.0) software. The t-test was used to compare differences between two groups. One-way or two-way analysis of variance (ANOVA) and Tukey' s multiple comparison tests were employed to analyze multiple parametric data sets. A significance level of $p < 0.05$ was used to determine statistical significance.

3 Results

3.1 ANPCD alleviates neurological dysfunction and pathological brain tissue damage in ICH rats

After modeling for 6 h, rats with intracerebral hemorrhage exhibited increased neurological deficit scores, which gradually decreased over time. The neurological function scores of drug-treated ICH rats declined rapidly, with the most significant decrease observed in rats treated with ANPCD. By 72 h, the ANPCD group had the lowest scores (Figure 1A). Nissl staining revealed that brain tissue surrounding the hemorrhage in the ICH group displayed edema, disordered cell arrangement, shrunken cell bodies, pyknotic nuclei, agglomeration and shrinkage of Nissl bodies, and a larger area of damage. In contrast, rats treated with ANPCD and ED showed reduced edema, mild cell damage, smaller damage area around the hemorrhage, with ANPCD demonstrating superior therapeutic effects compared to ED (Figure 1G).

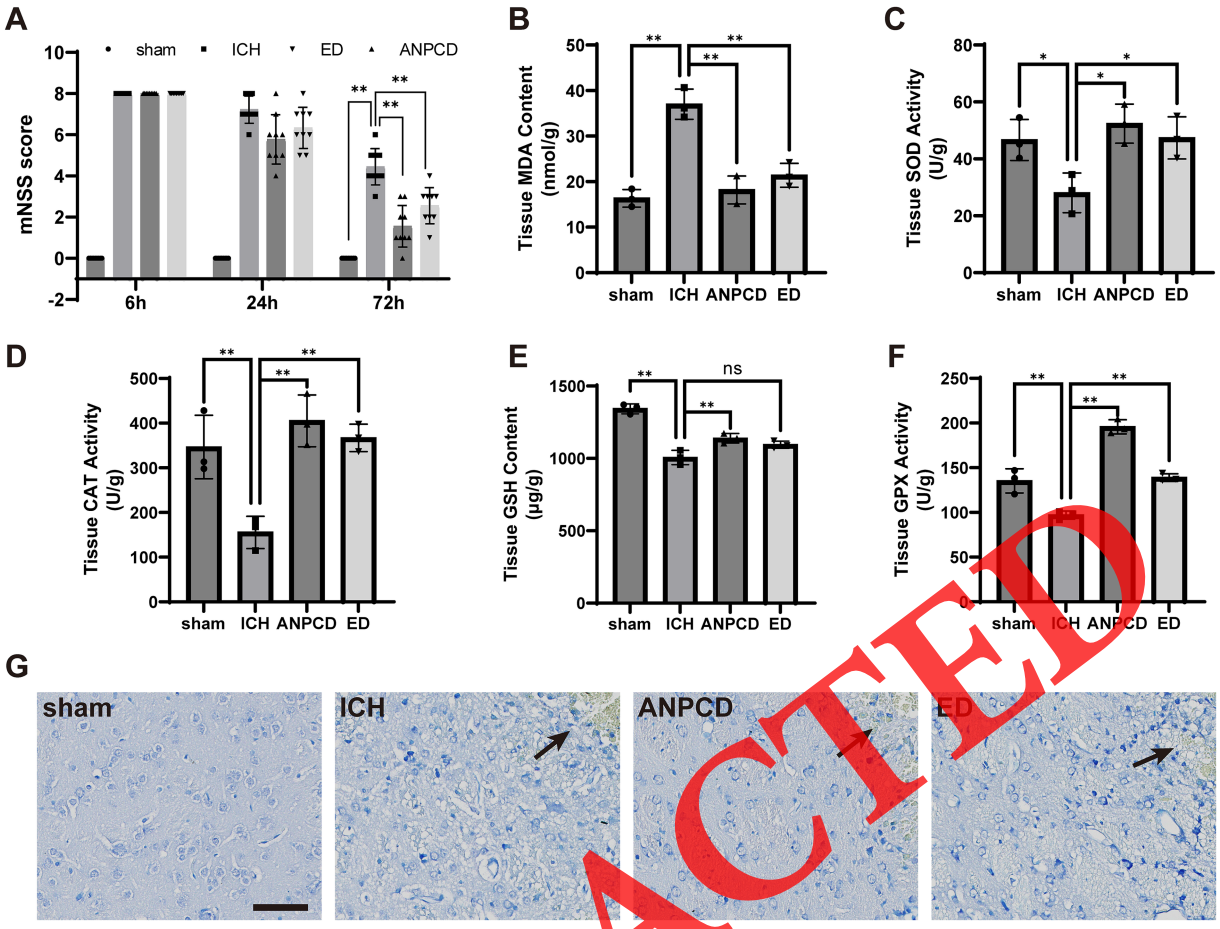

FIGURE 1
ANPCD alleviates neurological dysfunction and pathological brain tissue damage in ICH rats. **(A)** Neurological deficit scores after modelling in rats (n = 9). **(B–F)** Detection of oxidative stress product content and antioxidant enzyme activity in rat brain tissue (n = 3). **(G)** Nissl staining of rat brain sections, the position marked by the arrow is the location of the hemorrhage. Scale bar = 100 μm (200×). The data were subjected to analysis using the one-way or two-way ANOVA statistical technique. *, $P < 0.05$; **, $P < 0.01$. **(A)** $F = 441.4$, $p = 0.0001$; **(B)** $F = 34.35$, $p = 0.0001$; **(C)** $F = 6.793$, $p = 0.0137$; **(D)** $F = 14.03$, $p = 0.0015$; **(E)** $F = 45.26$, $p = 0.0001$; **(F)** $F = 69.79$, $p = 0.0001$.

3.2 ANPCD reduces oxidative stress levels in ICH rats

To assess the extent of oxidative stress following ICH in rats, we analyzed the concentration of oxidative stress markers, such as MDA, and the activity of antioxidant enzymes, including SOD, CAT, GSH, and GPX, in brain tissue surrounding the hemorrhage. The results demonstrated an increase in oxidative stress products and a decrease in antioxidant enzyme activity in ICH rats, indicating that oxidative stress in brain tissue was heightened in cerebral hemorrhage. Conversely, ANPCD and ED reversed this outcome, suggesting that ANPCD and ED could alleviate neuronal damage by reducing oxidative stress in brain tissue of ICH rats (Figures 1B–F).

3.3 ANPCD reduces the expression of NOX2, NOX4, and RAGE in brain tissue of ICH rats

We additionally analyzed the expression of NOX2, NOX4, and RAGE in brain tissue surrounding the hemorrhage in rats. Our results indicated that the expression of NOX2, NOX4, and RAGE was significantly higher in ICH rats compared to the sham group, and that NOX2, NOX4, and RAGE were decreased in both ANPCD and ED groups following drug treatment. This suggests that ANPCD may regulate oxidative stress in brain tissues of ICH rats by targeting NOX2, NOX4, and RAGE (Figures 2, 3).

3.4 ANPCD reduces neuronal cell apoptosis in ICH rats

Oxidative stress is a significant contributor to apoptosis. To investigate the impact of ICH on neuronal apoptosis in rats, we examined the expression of apoptosis-related protein in peri-hemorrhagic brain tissue. We found that the expression of Bax and CytoC was increased (Figures 4B,E), while the expression of Bcl-2 was decreased (Figure 4C), resulting in a significant increase in the Bax/Bcl-2 ratio (Figure 4D). Apoptosis rate was also elevated in peri-hemorrhagic nerve cells (Figures 4F,H). ANPCD and ED reversed these findings, indicating that they could effectively reduce neuronal cell apoptosis in brain tissue of ICH rats, thereby mitigating brain damage.

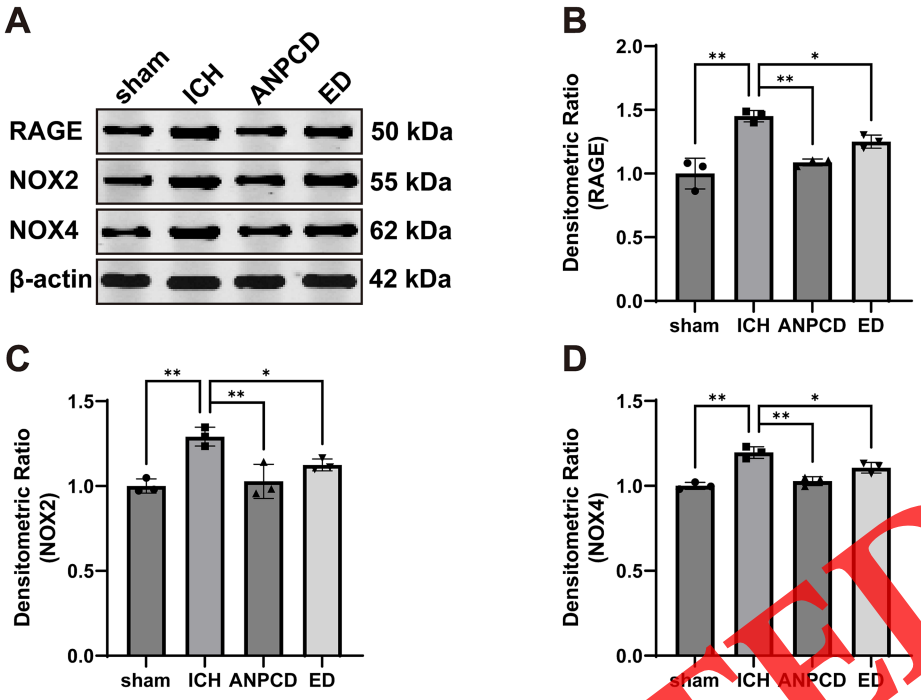

FIGURE 2
ANPCD reduces the expression of NOX2, NOX4, and RAGE in brain tissue of ICH rats. **(A–D)** Western blot analysis was employed to examine the protein expression of NOX2, NOX4 and RAGE (n = 3). The data were subjected to analysis using the one-way ANOVA statistical technique. *, $P < 0.05$. **, $P < 0.01$. **(B)** $F = 23.71$, $p = 0.0002$; **(C)** $F = 12.82$, $p = 0.0020$; **(D)** $F = 28.32$, $p = 0.0001$.

3.5 The quality control of ANPCD

Subsequently, prior to conducting cellular experiments, we analyzed the extracted drug-containing serum for its entry components and blood drug concentrations. By comparing these findings with the *in vitro* components of ANPCD identified in a previous study (Guo et al., 2023), we identified a total of 48 blood entry components, which included 13 flavonoids, 18 saponins, 10 terpenoids, 3 anthraquinones, and 4 additional compounds (Figures 5A,B). In addition, baicalin, baicalein, wogonin, oroxylin A, geniposide, genipin, crocin, rhein, emodin, rhynchophylline, isorhynchophylline, and hirsutine exhibit antioxidant activity (Zhou et al., 2024); geniposide, genipin, baicalin, and Paeoniflorin possess anti-inflammatory properties (Guo et al., 2023). A comprehensive list of ANPCD compounds that enter the bloodstream is presented in Supplementary Table S3. Notably, Baicalin, Wogonoside, and Geniposide have been reported to possess anti-oxidative properties that mitigate neurological damage (Cao et al., 2011; Zhang et al., 2014; Zou et al., 2020). We quantified their concentrations in the serum to assess the quality of the drug-containing serum, yielding the following results: Baicalin at 1.43 μg/mL, Wogonoside at 3.63 μg/mL, and Geniposide at 1.39 μg/mL, respectively (Figures 5C–E).

3.6 ANPCD-medicated serum attenuates neuronal damage by heme

To investigate how ANPCD mitigates oxidative stress in neurons following ICH, we employed heme to simulate the intra-tissue environment of cerebral hemorrhage and FPS-ZM1 to inhibit RAGE expression. Our findings indicated that heme induced extensive neuronal death, loss of neural networks, and cell lysis and fragmentation. Notably, blank serum was able to alleviate cell death, which manifested as significant neuronal network disruption. Following intervention with ANPCD-mediated serum and FPS-ZM1, neuronal integrity was substantially preserved, with a reduced number of cell deaths, intact cytosol, and only a few neuronal network breaks (Figures 6A,C). Results from the CCK-8 experiment demonstrated that cell viability in the blank serum group was higher than that in the normal group, suggesting a growth-promoting effect of the serum on neurons. In contrast, cell viability in the model group was significantly diminished; however, ANPCD-mediated serum and FPS-ZM1 effectively maintained high neuronal viability (Figure 6B). These findings suggest that ANPCD exhibits a robust neuroprotective effect, and the inhibition of RAGE also contributes to neuronal protection.

3.7 ANPCD-medicated serum attenuates heme-induced neuronal oxidative stress

To determine the effect of heme on neuronal oxidative stress injury, we analyzed the content of neuronal oxidative stress proxies such as ROS and MDA, as well as the activities of antioxidant enzymes including SOD, CAT, GSH, and GPX. Our results showed that heme significantly elevated the neuronal production of ROS and MDA, and simultaneously decreased the enzymatic activities of antioxidant enzymes. In contrast, ANPCD-medicated serum and FPS-ZM1

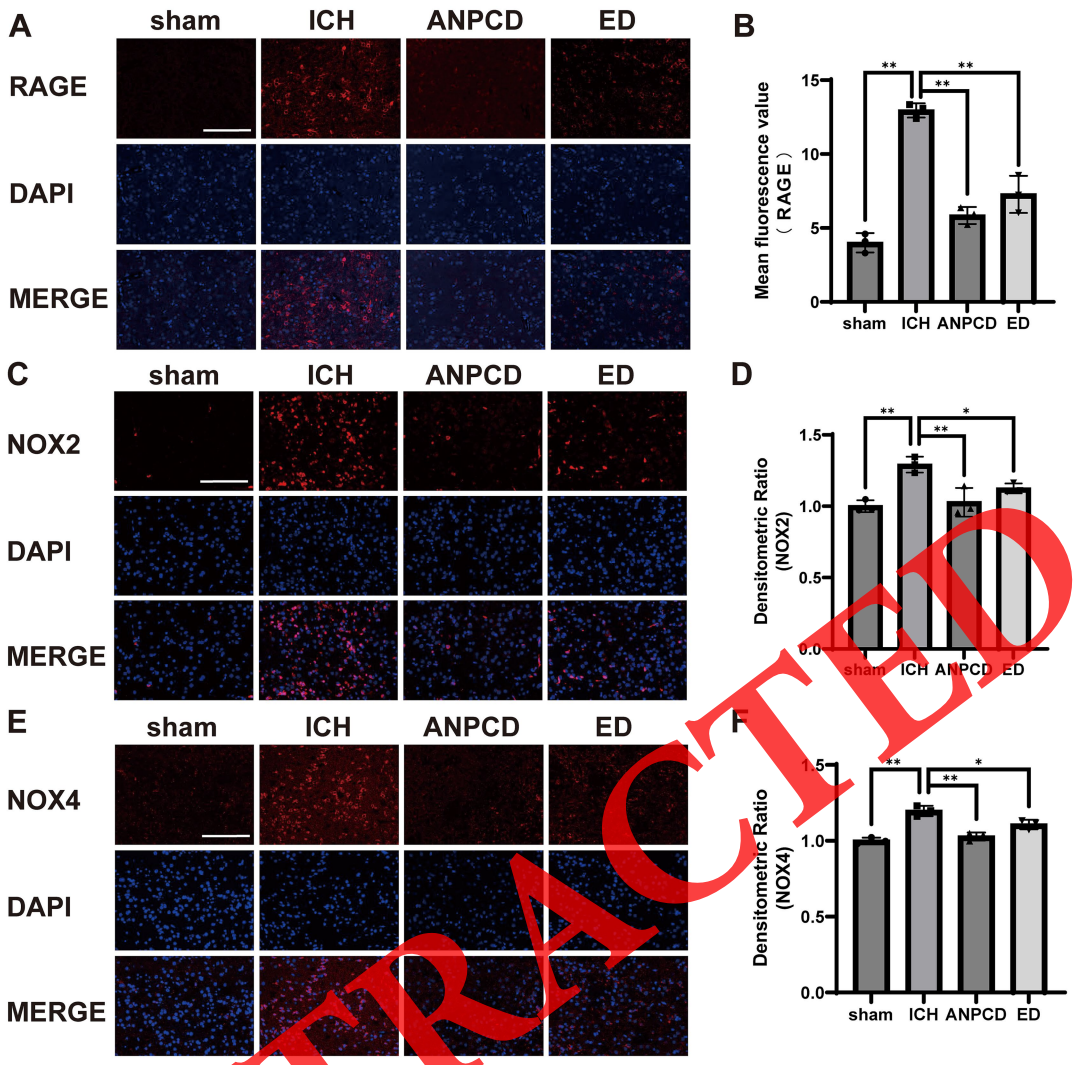

FIGURE 3
ANPCD reduces the expression of NOX2, NOX4, and RAGE in brain tissue of ICH rats. **(A–F)** Immunofluorescence assay analysis was employed to examine the protein expression of NOX2, NOX4 and RAGE (n = 3). Scale bar = 100 μm (200×). The data were subjected to analysis using the one-way ANOVA statistical technique. *, $P < 0.05$; **, $P \leq 0.01$. **(B)** $F = 69.57$, $p = 0.0001$; **(D)** $F = 67.84$, $p = 0.0001$; **(F)** $F = 20.27$, $p = 0.0004$.

reversed these effects, indicating that ANPCD-medicated serum intervention and inhibition of RAGE reduced the level of oxidative stress in heme-injured neurons (Figure 7).

3.8 ANPCD-medicated serum decreased NOX2, NOX4, and RAGE protein expression in heme-injured neurons

In addition, we analyzed the expression of NOX2, NOX4, and RAGE proteins. Our results showed that heme significantly increased the expression of these proteins in neurons. However, we observed a decrease in the expression of these proteins in neurons treated with ANPCD-mediated serum and FPS-ZM1. Our findings indicate that inhibition of RAGE reduced the expression of NOX2/4, and ANPCD-mediated serum also inhibited the heme-induced increase in neuronal NOX2, NOX4, and RAGE expression (Figures 8, 9).

3.9 ANPCD-medicated serum attenuated heme-induced neuronal apoptosis

We investigated neuronal apoptosis in the context of heme-induced injury. Our findings revealed a significant increase in the expression of apoptotic proteins Bax and CytoC (Figures 10B,E), accompanied by a reduction in the expression of the anti-apoptotic protein Bcl-2 (Figure 10C) in neurons of the model group. Furthermore, the Bax/Bcl-2 ratio and the rate of neuronal apoptosis were significantly elevated in this group (Figures 10D,F,G). Subsequently, we conducted fluorescence co-localization of mitochondria and CytoC in the cells. The results indicated that the fluorescence intensity of mitochondria in normal cells was higher than that of CytoC at the same localization. However, following hemin intervention, the fluorescence intensity of CytoC was significantly greater than that of mitochondria, possibly due to an increased content of CytoC in the cytoplasm (Figure 11). Notably, we found that ANPCD-mediated serum and FPS-ZM1 were able to reverse these

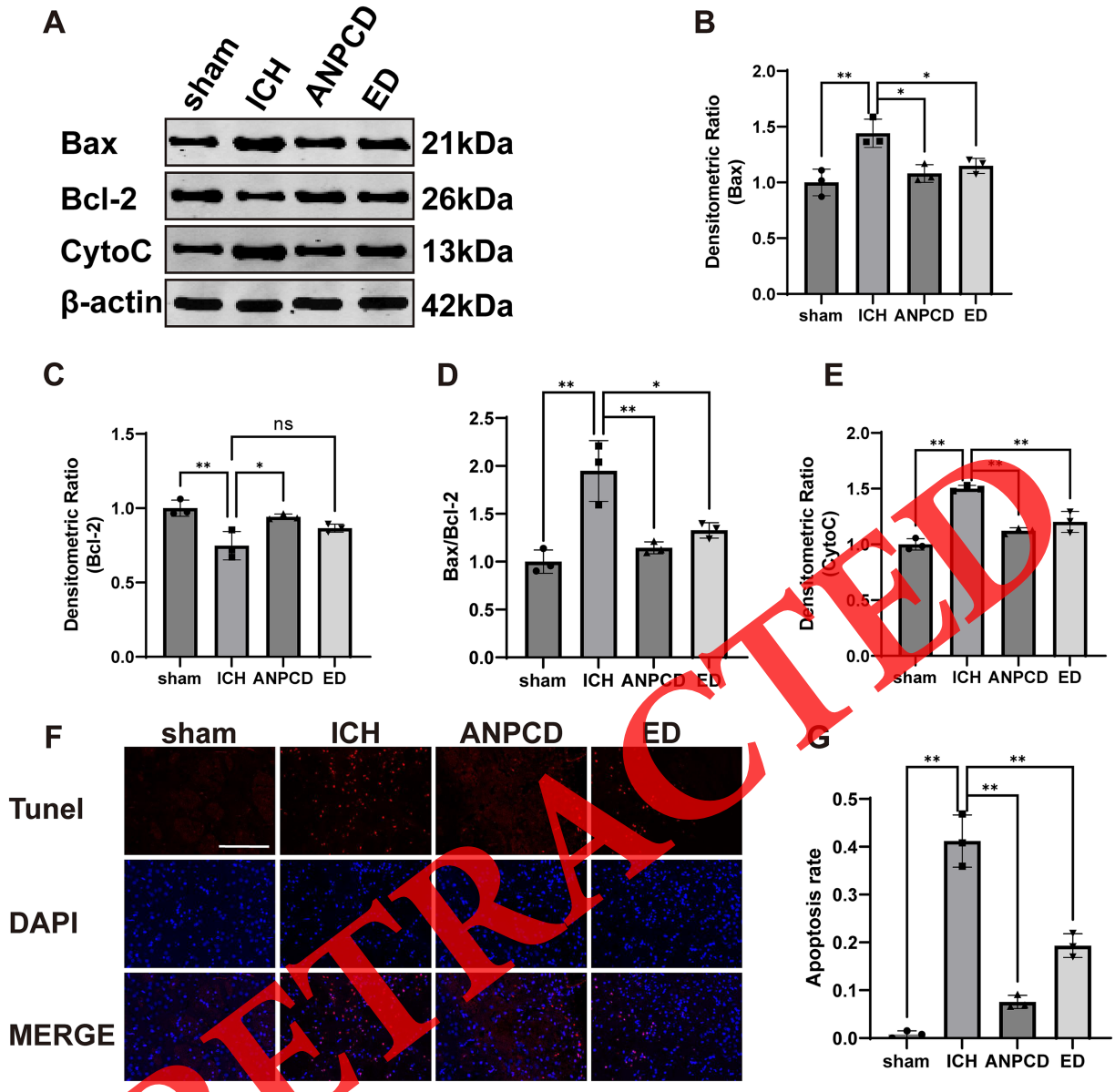

FIGURE 4
ANPCD reduces neuronal cell apoptosis in ICH rats. **(A–E)** Western blot analysis was employed to examine the protein expression of Bax, Bcl-2, and CytoC ($n = 3$). **(F,G)** TUNEL staining with fluorescence of brain tissue and apoptosis rate ($n = 3$). Scale bar = 100 μm (200×). The data were subjected to analysis using the one-way ANOVA statistical technique. *, $P < 0.05$. **, $P < 0.01$. **(B)** $F = 10.77$, $p = 0.0035$; **(C)** $F = 10.84$, $p = 0.0034$; **(D)** $F = 16.51$, $p = 0.0009$; **(E)** $F = 42.08$, $p = 0.0001$; **(G)** $F = 98.09$, $p = 0.0001$.

effects, suggesting that ANPCD can effectively reduce neuronal apoptosis and provide neuroprotection, while the inhibition of RAGE can also exert an anti-apoptotic effect.

4 Discussion

Oxidative stress-induced apoptosis is a key mechanism underlying neuronal death in SBI. Wang et al. (2018) demonstrated that in a rat model of ICH, significant oxidative stress and cellular apoptosis were evident in the brain tissue. Inhibiting oxidative stress has been shown to effectively ameliorate brain damage during SBI. In addition to directly damaging DNA, ROS-induced mitochondrial dysfunction is a major contributor to apoptosis. Impaired mitochondria elevate the expression of Bax and facilitate the formation of pores in the mitochondrial membrane, which promotes the release of CytoC from these pores (Trist et al., 2019). This process activates apoptotic signaling pathways involving caspase-9 and caspase-3, leading to the cleavage and degradation of specific intracellular proteins and nucleic acids, ultimately resulting in cell apoptosis (Li et al., 2022). The traditional Chinese medicine formula Buyang Huanwu Decoction is used for the treatment of stroke. It exhibits anti-apoptotic effects on neurons and alleviates brain damage following ICH through the ERK1/2 signaling pathway mediated by Sh2b3 (Cheng et al., 2024). In this study, pronounced oxidative stress and neuronal apoptosis were observed in the brains of ICH rats, which were associated with

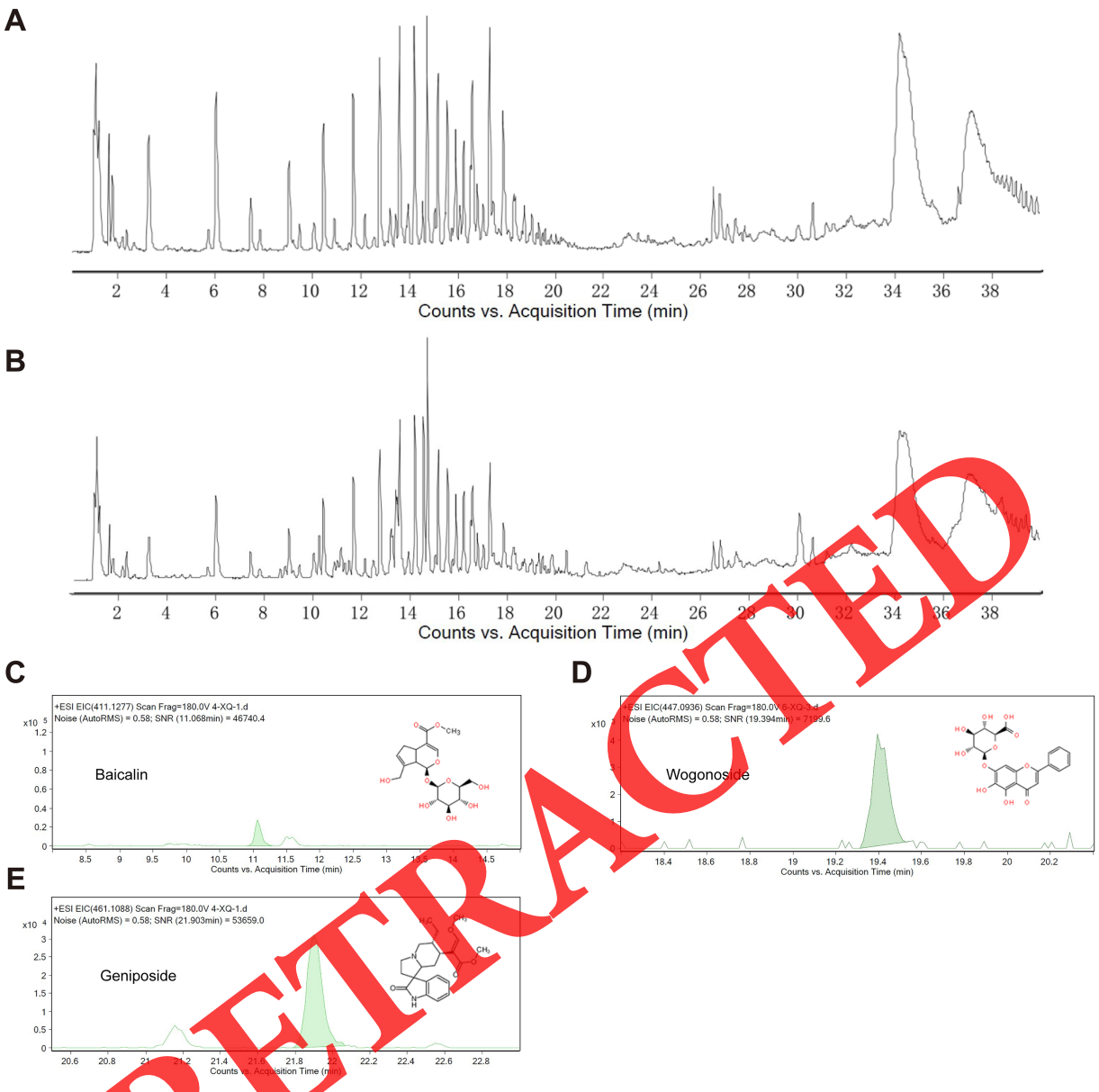

FIGURE 5
Characterization of QJHGD by UPLC-MS/MS. **(A)** Total ion current of blank serum. **(B)** Total ion current of ANPCD-medicated serum. **(C–E)** Qualitative analysis of 3 components.

diminished neurological function. Similar findings were obtained in cultured primary neurons. ANPCD exerts its neuroprotective effects by counteracting these detrimental processes.

Several drugs have been investigated for their potential to mitigate oxidative stress following ICH. Melatonin has been shown to reduce oxidative stress and neuronal apoptosis post-ICH by preserving mitochondrial function (Wang et al., 2018). Deferoxamine has demonstrated the ability to decrease oxidative stress and iron-induced cell death in neurons after ICH through the inhibition of ferritin deposition (Hatakeyama et al., 2013). However, the clinical efficacy of these drugs has yet to be established. ED is an oxygen free radical scavenger utilized in the clinical treatment of cerebral infarction. It can effectively penetrate brain tissue via the blood–brain barrier and eliminate ROS (Xu et al., 2022). Studies have indicated that this drug can also inhibit the oxidative stress response associated with ICH (Cao et al., 2023), which may enhance ICH-induced neurological deficits while reducing brain edema, oxidative damage, and brain injury caused by iron and thrombin (Nakamura et al., 2008).

Antioxidant enzymes represent a crucial class of enzymes that safeguard cells against oxidative damage. SOD functions by scavenging superoxide radicals, whereas CAT and GPX contribute by removing hydrogen peroxide, thereby exerting their antioxidant effects. MDA is a highly reactive metabolite produced during lipid peroxidation and is widely regarded as a key indicator of oxidative stress and cellular damage. MDA can interact with proteins, DNA, and other biomolecules, resulting in oxidative damage to cell membranes and compromised cellular function (Bu et al., 2021). Our study demonstrated that both ANPCD and ED enhanced the

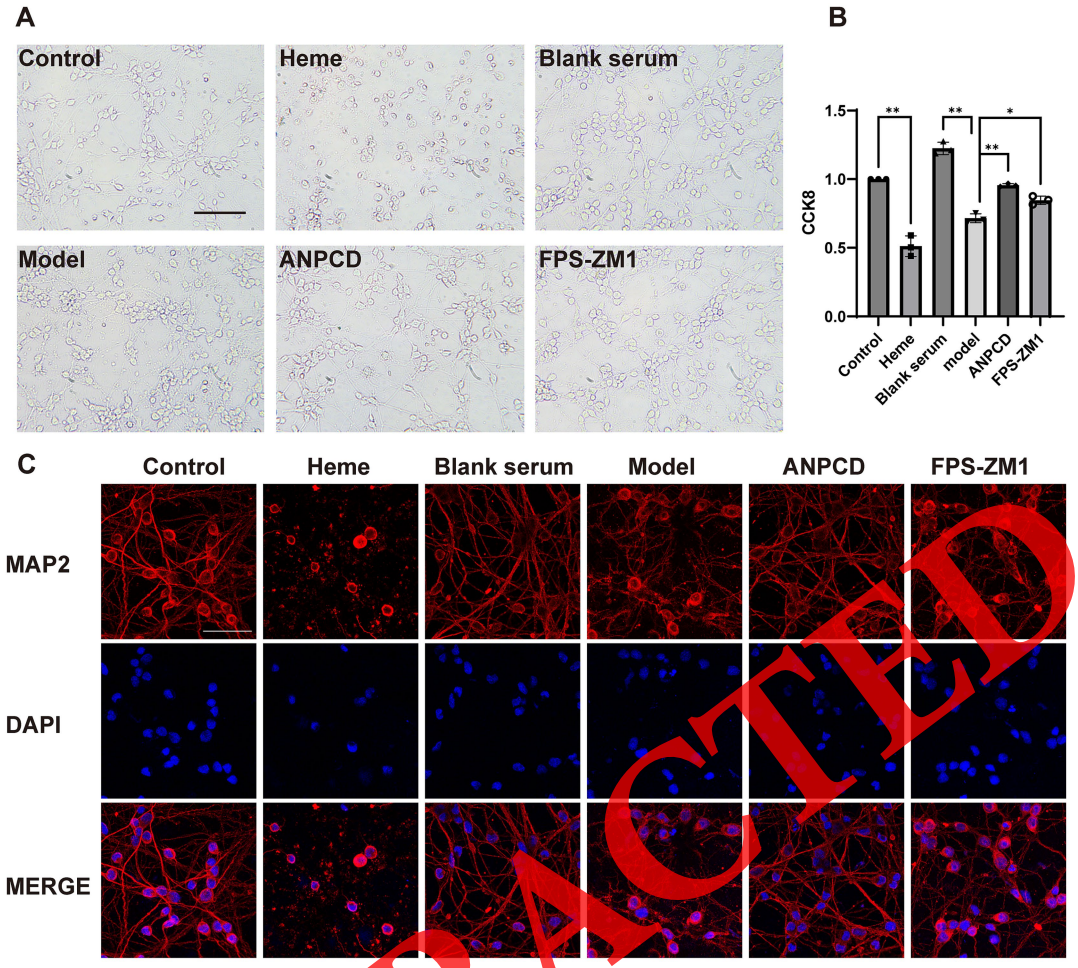

FIGURE 6
ANPCD-medicated serum attenuates neuronal damage by heme. (A) Bright field photographs of primary neurons. Scale bar = 100 μm (200×). **(B)** The viability of primary neurons was assessed using a CCK-8 assay (n = 3). **(C)** The observation of neuronal networks was conducted using immunofluorescent labelling of neuronal MAP2 protein. Scale bar = 50 μm (400×). The data were subjected to analysis using the one-way ANOVA statistical technique. *, $P < 0.05$. **, $P < 0.01$. **(B)** $F = 111.6$, $p = 0.0001$.

activities of SOD, CAT, and GPX, while simultaneously reducing levels of MDA and ROS. Interestingly, ANPCD exhibits superior efficacy compared to ED in reducing oxidative stress levels and providing neuroprotection in the brain tissue of rats with ICH. ANPCD consists of 10 botanical drugs and 2 mineral drugs. Among the 48 blood-entering compounds previously identified, numerous compounds demonstrate antioxidant effects through various targets. For example, paeoniflorin (Wang et al., 2022), baicalin (Xu et al., 2013), rhynchophylline (Zhang et al., 2016), and glycyrrhizic acid (Zhu et al., 2022) can alleviate brain damage caused by stroke by diminishing oxidative stress in brain tissue. The multifaceted mechanisms through which herbal compounds exert their efficacy by targeting multiple pathways and molecular targets may primarily explain the enhanced effectiveness of ANPCD over ED. In addition to mitigating oxidative stress, ANPCD also reduces inflammation levels in the brain, thereby achieving improved efficacy.

Heme is identified as one of the ligands of RAGE (Yepuri et al., 2021). It has been suggested that NOX may serve as a downstream target of the oxidative stress induced by RAGE (Piras et al., 2016; Ray et al., 2016). NOX is capable of catalyzing the conversion of oxygen into superoxide and performs various functions, including host defense, post-translational processing of proteins, cell signaling, gene expression regulation, and cell differentiation (Vermot et al., 2021). NOX2 and NOX4 are predominantly located on the cell membrane. When external factors such as heme and hemoglobin interact with neurons, the receptors on the cell membrane are the first to be activated. However, these external factors do not directly interact with the NOX2 and NOX4 proteins, as the majority of these proteins reside within the cell membrane and are involved in intracellular oxidation reactions. Consequently, the RAGE receptor plays a crucial intermediary role. Under normal conditions, RAGE expression is minimal; however, upon exposure to external substances, its expression levels increase. The activated RAGE transmits signals to NOX, thereby enhancing its activity (Moreira et al., 2022). It has been observed that the application of RAGE inhibitors can effectively decrease the expression of NOX2 and NOX4 proteins. The activation of the RAGE-NOX2/4 signaling pathway may represent a significant source of ROS during the initial stages of neuronal damage following ICH.

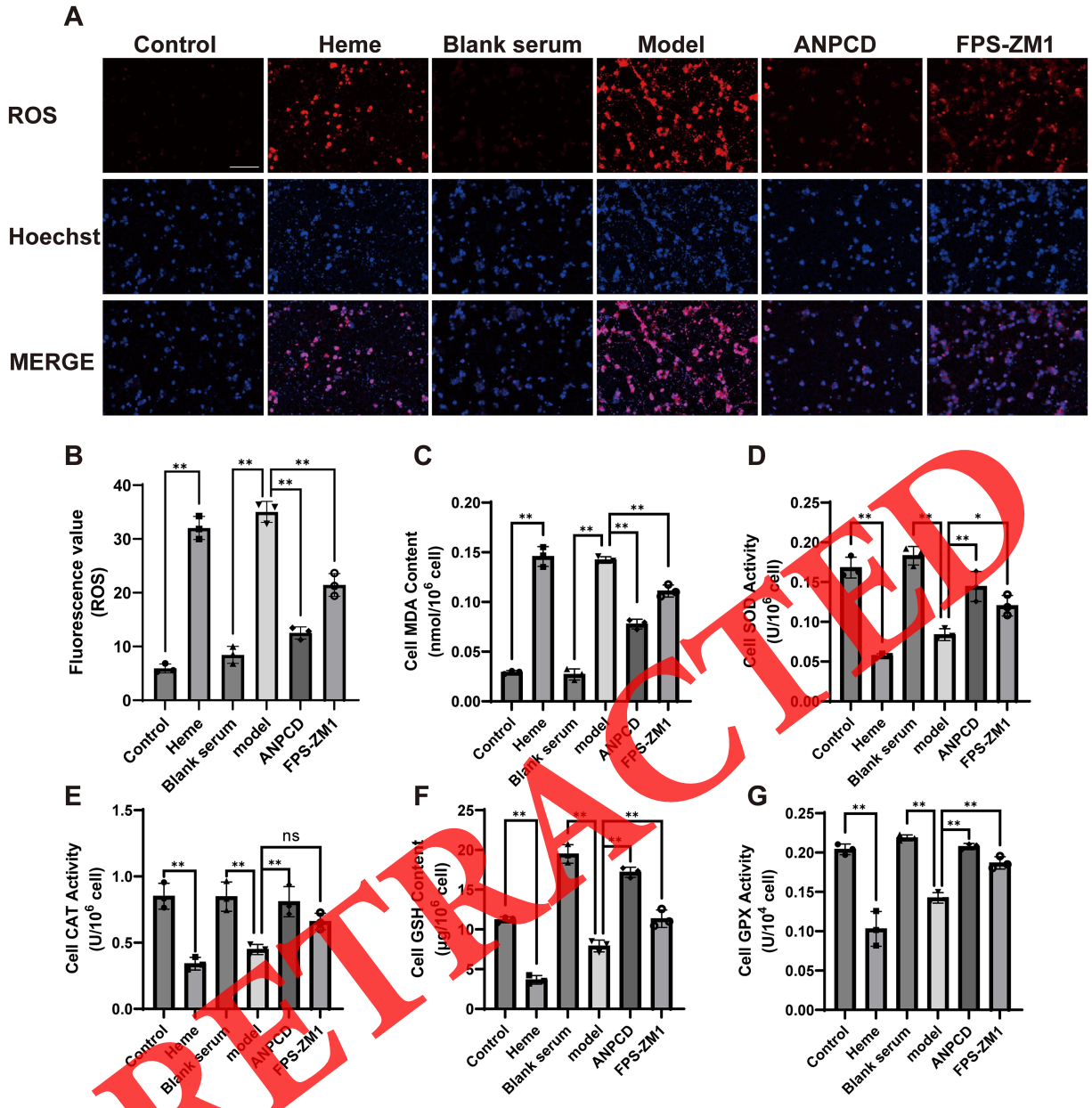

FIGURE 7
ANPCD-medicated serum attenuates heme-induced neuronal oxidative stress. **(A,B)** Fluorescence detection of ROS in primary neurons (n = 3). Scale bar = 100 μm (100×). **(C–G)** Detection of oxidative stress product content and antioxidant enzyme activity in primary neurons (n = 3). The data were subjected to analysis using the one-way ANOVA statistical technique. *, $P < 0.05$. **, $P < 0.01$. **(B)** $F = 157.2$, $p = 0.0001$; **(C)** $F = 246.4$, $p = 0.0001$; **(D)** $F = 47.92$, $p = 0.0001$; **(E)** $F = 20.38$, $p = 0.0001$; **(F)** $F = 154.7$, $p = 0.0001$; **(G)** $F = 54.98$, $p = 0.0001$.

Mitochondrial dysfunction is a significant source of intracellular oxidative stress. Researchers have proposed the "ROS induces ROS" theory, which posits that excessive ROS within cells disrupts normal mitochondrial function, leading to increased ROS production and creating a detrimental positive feedback loop (Fukai and Ushio-Fukai, 2020). Unlike the RAGE-activated NOX pathway for ROS production, mitochondrial ROS generation is an endogenous process, with mitochondrial dysfunction serving as a prerequisite for this phenomenon (Sarniak et al., 2016), while RAGE can be directly activated by external stimuli. Consequently, the initial source of ROS that induces mitochondrial dysfunction may arise from heightened NOX activity. Notably, NOX4 is also localized on the membranes of mitochondria, the endoplasmic reticulum, and other organelles (Wang et al., 2023). NOX4 can directly influence mitochondrial function and plays a regulatory role in intracellular ROS production. Yang et al. (2015) found that the signal transduction pathways associated with RAGE following ICH contribute to damage of the blood–brain barrier and white matter fibers, with the initiation of this signaling linked to iron ions. The application of RAGE antagonists has been shown to effectively mitigate early brain damage after ICH. Additionally, Ding et al. (2023) demonstrated that employing NOX4 adeno-associated virus knockdown in rats enhances neuronal tolerance to oxidative stress post-ICH, reduces mitochondrial ROS production, alleviates mitochondrial damage, and inhibits the

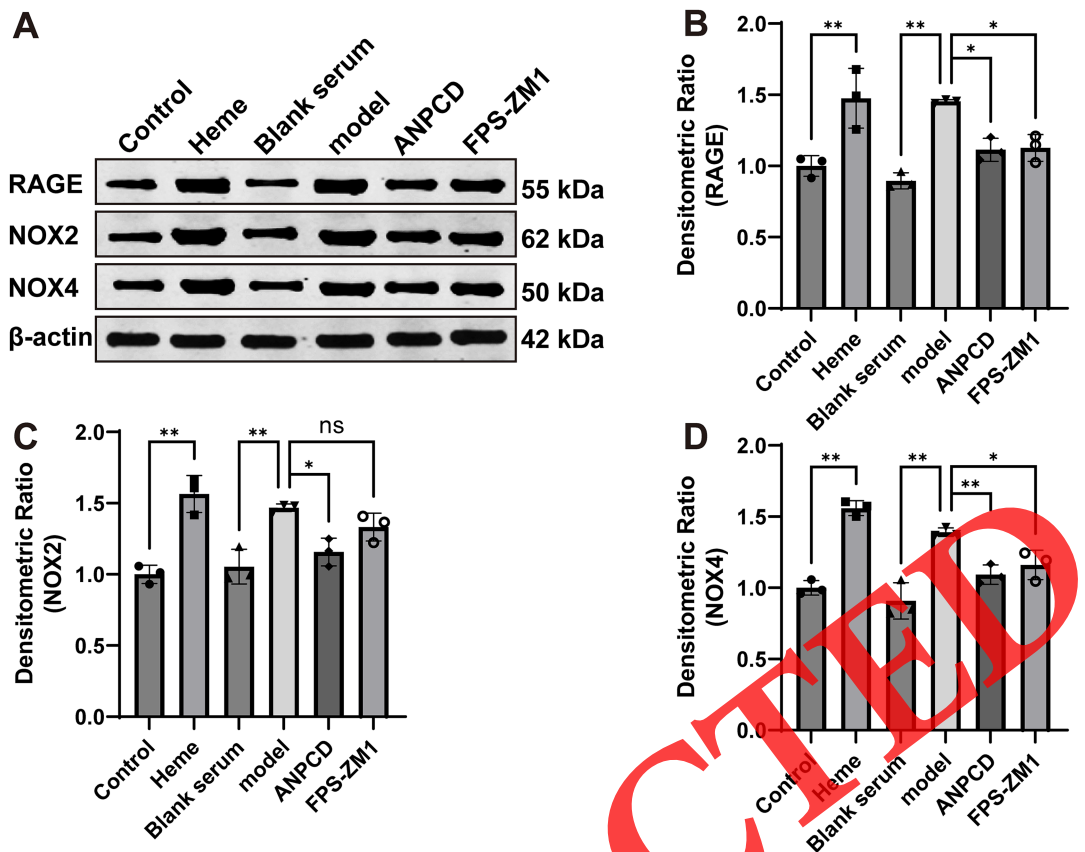

FIGURE 8
ANPCD-medicated serum decreased NOX2, NOX4, and RAGE protein expression in heme-injured neurons. **(A–D)** Western blot analysis was employed to examine the protein expression of NOX2, NOX4 and RAGE ($n = 3$). The data were subjected to analysis using the one-way ANOVA statistical technique. *, $P < 0.05$. **, $P < 0.01$. **(B)** $F = 14.92$, $p = 0.0001$; **(C)** $F = 16.97$, $p = 0.0001$; **(D)** $F = 28.60$, $p = 0.0001$.

progression of SBI after ICH. Thus, preventing the overactivation of NOX2/4 enzymes represents a promising strategy to counteract neuronal oxidative stress and mitochondrial dysfunction following ICH. Investigating the effects of ANPCD on neuronal mitochondrial function after ICH will be a primary focus of our upcoming studies.

In previous studies, we employed network pharmacology methods to investigate the SIRT1 gene and briefly elucidated its impact on oxidative stress following ICH. However, the role of SIRT1 extends beyond mere alterations in intracellular oxidative stress. SIRT1 is significantly involved in mitochondrial biogenesis and the maintenance of mitochondrial functional homeostasis. Research has demonstrated that SIRT1 can regulate downstream targets such as PGC-1α, FOXO, and NRF2, thereby modulating mitochondrial biogenesis and function (Tang, 2016), which are crucial for neuronal neurite and synaptic regeneration, as well as normal neuronal signal transmission following ICH (Cardanho-Ramos and Morais, 2021). Nonetheless, oxidative stress remains an unavoidable intermediate step in these processes. Consequently, unlike previous studies that focused on serum samples, this study obtained brain tissue samples after ICH and conducted both animal and cell experiments to comprehensively investigate the changes in neuronal oxidative stress following ICH. This approach lays the groundwork for further research on the impact of SIRT1 on mitochondrial and synaptic regeneration.

In conclusion, we observed an increase in the expression of RAGE and NOX2/4, along with a phenomenon of oxidative stress, following ICH in rats. The intervention of primary neurons with heme demonstrated that the RAGE receptor blocker FPS-ZM1 effectively prevented NOX2/4 from generating oxidative stress. Furthermore, treatment with ANPCD can significantly inhibit the activation of the RAGE-NOX2/4 signaling axis, thereby mitigating oxidative stress damage to neurons after ICH. However, there are some limitations in this study. On one hand, while there is additional evidence supporting RAGE as one of the upstream targets of NOX, the specific mechanisms underlying NOX activation by RAGE remain unclear, and further investigation is required to elucidate these processes. On the other hand, mitochondria are closely related to oxidative stress, and this study lacks further exploration of the connection between the RAGE-NOX2/4 signaling axis and mitochondria.

Data availability statement

The original contributions presented in the study are included in the article/Supplementary material, further inquiries can be directed to the corresponding authors.

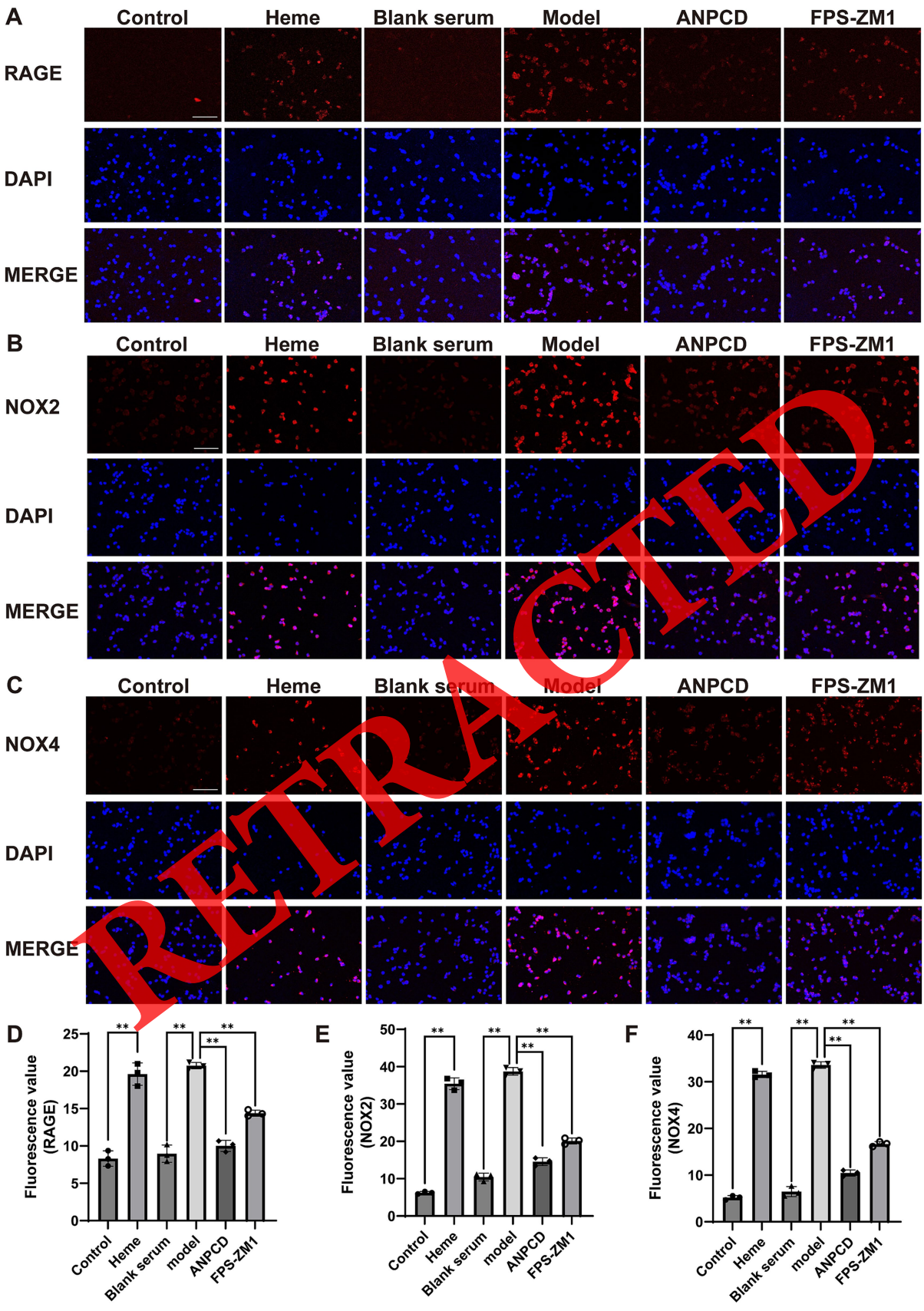

FIGURE 9
ANPCD-medicated serum decreased NOX2, NOX4, and RAGE protein expression in heme-injured neurons. **(A–F)** Immunofluorescence assay analysis was employed to examine the protein expression of NOX2, NOX4 and RAGE (n = 3). Scale bar = 100 μm (100×). The data were subjected to analysis using the one-way ANOVA statistical technique. *, $P < 0.05$. **, $P < 0.01$. **(D)** $F = 97.86$, $p = 0.0001$; **(E)** $F = 493.3$, $p = 0.0001$; **(F)** $F = 907.2$, $p = 0.0001$.

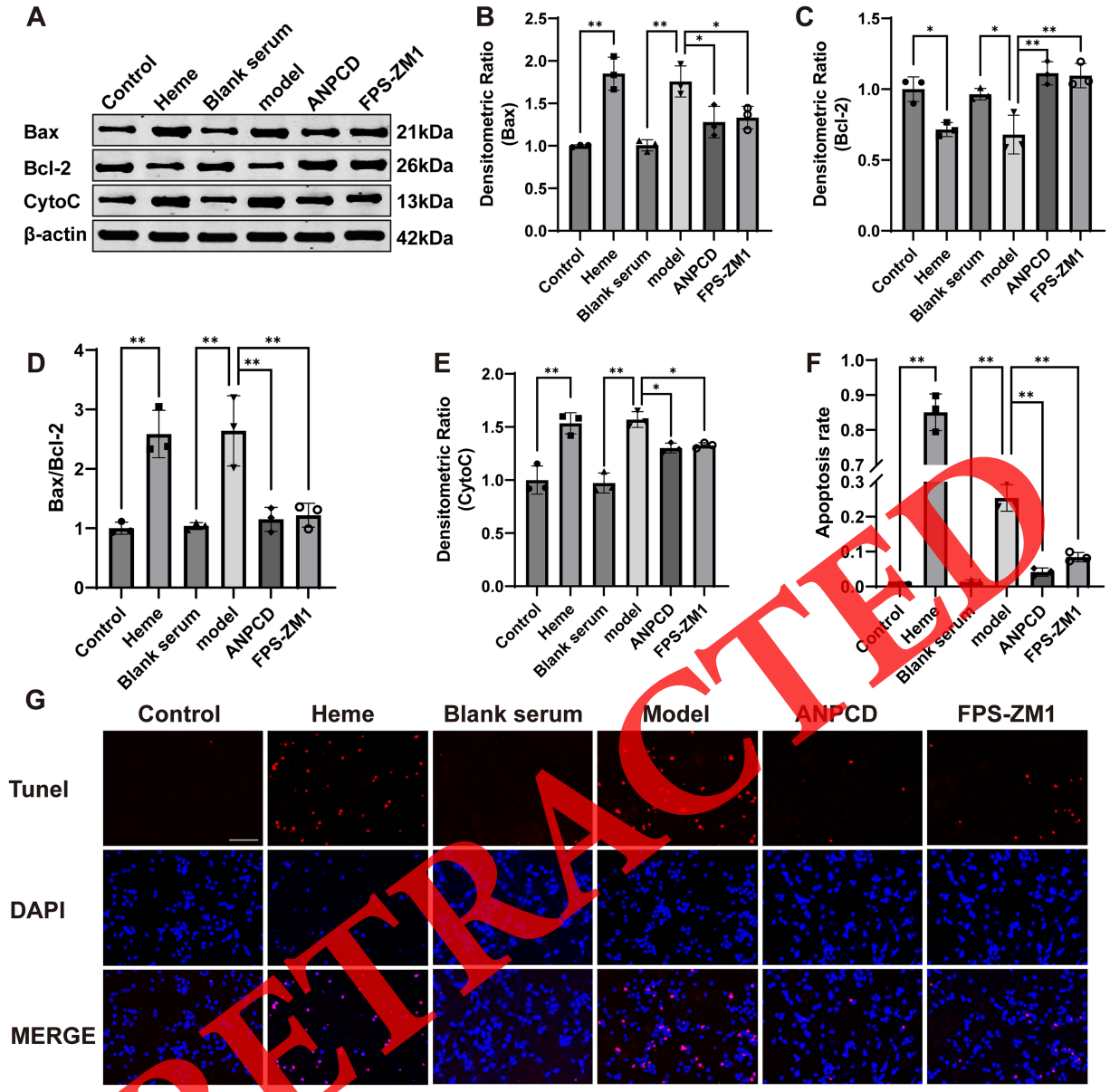

FIGURE 10
ANPCD-medicated serum attenuated heme-induced neuronal apoptosis. **(A–E)** Western blot analysis was employed to examine the protein expression of Bax, Bcl-2, and CytoC (n = 3). **(F,G)** TUNEL staining with fluorescence of primary neurons and apoptosis rate (n = 3). Scale bar = 100 μm (100×). The data were subjected to analysis using the one-way ANOVA statistical technique. *, $P < 0.05$. **, $P < 0.01$. **(B)** $F = 18.65$, $p = 0.0001$; **(C)** $F = 14.24$, $p = 0.0001$; **(D)** $F = 18.32$, $p = 0.0001$; **(E)** $F = 25.92$, $p = 0.0001$; **(F)** $F = 426.6$, $p = 0.0001$.

Ethics statement

The animal study was approved by Ethics Committee for Experimental Animals of the First Hospital of the Hunan University of Chinese Medicine (Approval No.: ZYFY20231101-98). The study was conducted in accordance with the local legislation and institutional requirements.

Author contributions

XW: Conceptualization, Data curation, Formal analysis, Methodology, Validation, Visualization, Writing – original draft, Writing – review & editing. XL: Conceptualization, Formal analysis, Methodology, Writing – original draft, Writing – review & editing. ZC: Formal analysis, Methodology, Writing – original draft, Writing – review & editing. HL: Formal analysis, Software, Validation, Writing – original draft, Writing – review & editing. XZ: Methodology, Writing – original draft, Writing – review & editing. SL: Methodology, Validation, Writing – original draft, Writing – review & editing. JL: Methodology, Writing – original draft, Writing – review & editing. HD: Methodology, Writing – original draft, Writing – review & editing. FL: Writing – original draft, Writing – review & editing. HH: Methodology, Supervision, Writing – original draft, Writing – review & editing. CG: Conceptualization, Data curation, Funding acquisition,

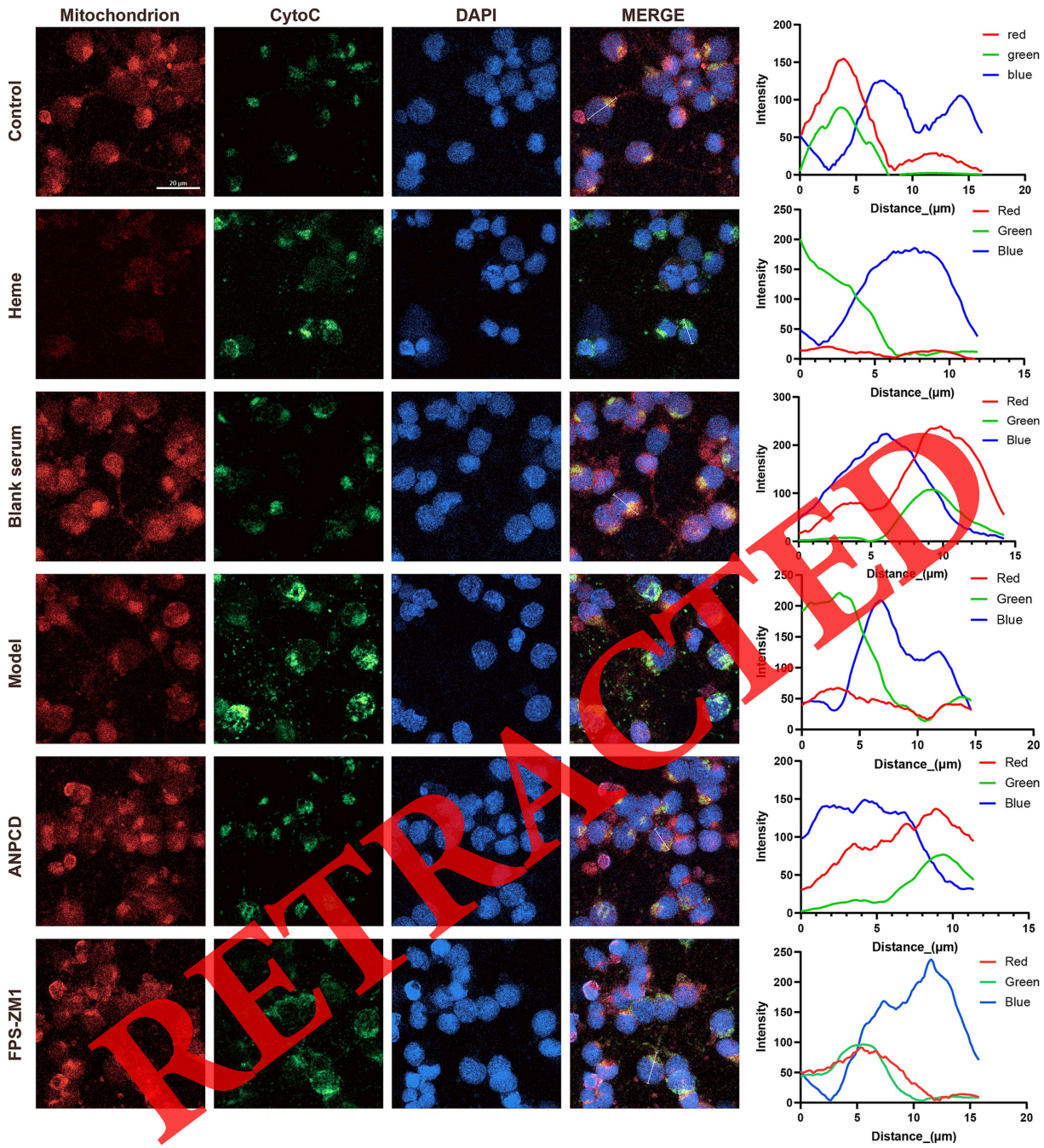

FIGURE 11
Line graph showing the fluorescence intensity of mitochondria and CytoC co-localization in representative cells. The red line represents mitochondria, the green line represents CytoC, and the blue line represents the cell nucleus (n = 3). Scale bar = 20 μm (400×).

Methodology, Project administration, Supervision, Writing – original draft, Writing – review & editing.

Funding

The author(s) declare that financial support was received for the research, authorship, and/or publication of this article. This work was supported by the National Natural Science Foundation of China (Grant no. 81874463), Natural Science Foundation of Hunan Province (Grant no. 2024JJ5316), Health Research Project of Hunan Provincial Health Commission (Grant no. W20242018) and Natural Science Foundation of Changsha (Grant no. Kq2208208).

Acknowledgments

We thank the Experimental Center of Medical Innovation of The First Hospital of Hunan University of Chinese Medicine for providing the experimental conditions.

Conflict of interest

The authors declare that the research was conducted in the absence of any commercial or financial relationships that could be construed as a potential conflict of interest.

Publisher's note

All claims expressed in this article are solely those of the authors and do not necessarily represent those of their affiliated organizations, or those of the publisher, the editors and the reviewers. Any product that may be evaluated in this article, or claim that may be made by its manufacturer, is not guaranteed or endorsed by the publisher.

Supplementary material

The Supplementary material for this article can be found online at: https://www.frontiersin.org/articles/10.3389/fnins.2024.1491343/full#supplementary-material

References

Bautista, W., Adelson, P. D., Bicher, N., Themistocleous, M., Tsivgoulis, G., and Chang, J. J. (2021). Secondary mechanisms of injury and viable pathophysiological targets in intracerebral hemorrhage. *Ther. Adv. Neurol. Disord.* 14:17562864211049208. doi: 10.1177/17562864211049208

Bu, R., Yan, B., Sun, H., Zhou, M., Bai, H., Cai, X., et al. (2021). Copper tolerance mechanism of the novel marine multi-stress tolerant yeast *Meyerozyma guilliermondii* GXDK6 as revealed by integrated omics analysis. *Front. Microbiol.* 12:771878. doi: 10.3389/fmicb.2021.771878

Cao, Y., Mao, X., Sun, C., Zheng, P., Gao, J., Wang, X., et al. (2011). Baicalin attenuates global cerebral ischemia/reperfusion injury in gerbils via anti-oxidative and anti-apoptotic pathways. *Brain Res. Bull.* 85, 396–402. doi: 10.1016/j.brainresbull.2011.05.002

Cao, S., Wei, J., Cai, Y., Xiong, Z., Li, J., Jiang, Z., et al. (2023). Network pharmacology prediction and experimental verification for anti-Ferroptosis of Edaravone after experimental intracerebral hemorrhage. *Mol. Neurobiol.* 60, 3633–3649. doi: 10.1007/s12035-023-03279-x

Cardanho-Ramos, C., and Morais, V. A. (2021). Mitochondrial biogenesis in neurons: how and where. *Int. J. Mol. Sci.* 22:13059. doi: 10.3390/ijms222313059

Chen, Y., Chen, S., Chang, J., Wei, J., Feng, M., and Wang, R. (2021). Perihematomal edema after intracerebral hemorrhage: An update on pathogenesis, risk factors, and therapeutic advances. *Front. Immunol.* 12:740632. doi: 10.3389/fimmu.2021.740632

Cheng, M., Li, T., Hu, E., Yan, Q., Li, H., Wang, Y., et al. (2024). A novel strategy of integrating network pharmacology and transcriptome reveals antiapoptotic mechanisms of Buyang Huanwu decoction in treating intracerebral hemorrhage. *J. Ethnopharmacol.* 319:117123. doi: 10.1016/j.jep.2023.117123

Ding, H., Li, Y., Chen, S., Wen, Y., Zhang, S., Luo, E., et al. (2022). Fisetin ameliorates cognitive impairment by activating mitophagy and suppressing neuroinflammation in rats with sepsis-associated encephalopathy. *CNS Neurosci. Ther.* 28, 247–258. doi: 10.1111/cns.13765

Ding, B. Y., Xie, C. N., Xie, J. Y., Gao, Z. W., Fei, X. W., Hong, E. H., et al. (2023). Knockdown of NADPH oxidase 4 reduces mitochondrial oxidative stress and neuronal pyroptosis following intracerebral hemorrhage. *Neural Regen. Res.* 0–1742. doi: 10.4103/1673-5374.360249

Fukai, T., and Ushio-Fukai, M. (2020). Cross-talk between NADPH oxidase and mitochondria: role in ROS signaling and angiogenesis. *Cells* 9:1849. doi: 10.3390/cells9081849

Guo, C., Zhou, X., Wang, X., Wang, H., Liu, J., Wang, J., et al. (2023). Annao Pingchong decoction alleviate the neurological impairment by attenuating neuroinflammation and apoptosis in intracerebral hemorrhage rats. *J. Ethnopharmacol.* 310:116298. doi: 10.1016/j.jep.2023.116298

Hatakeyama, T., Okauchi, M., Hua, Y., Keep, R. F., and Xi, G. (2013). Deferoxamine reduces neuronal death and hematoma lysis after intracerebral hemorrhage in aged rats. *Transl. Stroke Res.* 4, 546–553. doi: 10.1007/s12975-013-0270-5

Li, Y., Liu, H., Tian, C., An, N., Song, K., Wei, Y., et al. (2022). Targeting the multifaceted roles of mitochondria in intracerebral hemorrhage and therapeutic prospects. *Biomed. Pharmacother.* 148:112749. doi: 10.1016/j.biopha.2022.112749

Moreira, A. P., Vizuete, A., Zin, L., de Marques, C. O., Pacheco, R. F., Leal, M. B., et al. (2022). The methylglyoxal/RAGE/NOX-2 pathway is persistently activated in the Hippocampus of rats with STZ-induced sporadic Alzheimer's disease. *Neurotox. Res.* 40, 395–409. doi: 10.1007/s12640-022-00476-9

Nakamura, T., Kuroda, Y., Yamashita, S., Zhang, X., Miyamoto, O., Tamiya, T., et al. (2008). Edaravone attenuates brain edema and neurologic deficits in a rat model of acute intracerebral hemorrhage. *Stroke* 39, 463–469. doi: 10.1161/STROKEAHA.107.486654

Piras, S., Furfaro, A. L., Domenicotti, C., Traverso, N., Marinari, U. M., Pronzato, M. A., et al. (2016). RAGE expression and ROS generation in neurons: differentiation versus damage. *Oxidative Med. Cell. Longev.* 2016:9348651. doi: 10.1155/2016/9348651

Ray, R., Juranek, J. K., and Rai, V. (2016). RAGE axis in neuroinflammation, neurodegeneration and its emerging role in the pathogenesis of amyotrophic lateral sclerosis. *Neurosci. Biobehav. Rev.* 62, 48–55. doi: 10.1016/j.neubiorev.2015.12.006

Ren, H., Han, R., Chen, X., Liu, X., Wan, J., Wang, L., et al. (2020). Potential therapeutic targets for intracerebral hemorrhage-associated inflammation: An update. *J. Cereb. Blood Flow Metab.* 40, 1752–1768. doi: 10.1177/0271678X20923551

Rendevski, V., Aleksovski, B., Mihajlovska Rendevska, A., Hadzi-Petrushev, N., Manusheva, N., Shuntov, B., et al. (2023). Inflammatory and oxidative stress markers in intracerebral hemorrhage: relevance as prognostic markers for quantification of the edema volume. *Brain Pathol.* 33:e13106. doi: 10.1111/bpa.13106

Sarniak, A., Lipińska, J., Tytman, K., and Lipińska, S. (2016). Endogenous mechanisms of reactive oxygen species (ROS) generation. *Postepy Higieny Medycyny Doswiadczalnej* 70, 1150–1165. doi: 10.5604/17322693.1224259

Shadfar, S., Parakh, S., Jamali, M. S., and Atkin, J. D. (2023). Redox dysregulation as a driver for DNA damage and its relationship to neurodegenerative diseases. *Transl. Neurodegener.* 12:18. doi: 10.1186/s40035-023-00350-4

Tang, B. L. (2016). Sirt1 and the mitochondria. *Mol. Cells* 39, 87–95. doi: 10.14348/molcells.2016.2318

Terzi, A., and Suter, D. M. (2020). The role of NADPH oxidases in neuronal development. *Free Radic. Biol. Med.* 154, 33–47. doi: 10.1016/j.freeradbiomed.2020.04.027

Trist, B. G., Hare, D. J., and Double, K. L. (2019). Oxidative stress in the aging substantia nigra and the etiology of Parkinson's disease. *Aging Cell* 18:e13031. doi: 10.1111/acel.13031

Vermot, A., Petit-Härtlein, I., Smith, S., and Fieschi, F. (2021). NADPH oxidases (NOX): An overview from discovery, molecular mechanisms to physiology and pathology. *Antioxidants* 10:890. doi: 10.3390/antiox10060890

Wang, D., Li, J., Luo, G., Zhou, J., Wang, N., Wang, S., et al. (2023). Nox4 as a novel therapeutic target for diabetic vascular complications. *Redox Biol.* 64:102781. doi: 10.1016/j.redox.2023.102781

Wang, P. C., Wang, S. X., Yan, X. L., He, Y. Y., Wang, M. C., Zheng, H. Z., et al. (2022). Combination of paeoniflorin and calycosin-7-glucoside alleviates ischaemic stroke injury via the PI3K/AKT signalling pathway. *Pharm. Biol.* 60, 1469–1477. doi: 10.1080/13880209.2022.2102656

Wang, Z., Zhou, F., Dou, Y., Tian, X., Liu, C., Li, H., et al. (2018). Melatonin alleviates intracerebral hemorrhage-induced secondary brain injury in rats via suppressing apoptosis, inflammation, oxidative stress, DNA damage, and mitochondria injury. *Transl. Stroke Res.* 9, 74–91. doi: 10.1007/s12975-017-0559-x

Wu, X., Jiao, W., Chen, J., Tao, Y., Zhang, J., and Wang, Y. (2022). Ulinastatin alleviates early brain injury after intracerebral hemorrhage by inhibiting oxidative stress and neuroinflammation via ROS/MAPK/Nrf2 signaling pathway. *Acta Cir. Bras.* 37:e370606. doi: 10.1590/acb370606

Xie, J., Hong, E., Ding, B., Jiang, W., Zheng, S., Xie, Z., et al. (2020). Inhibition of NOX4/ROS suppresses neuronal and blood-brain barrier injury by attenuating oxidative stress after intracerebral hemorrhage. *Front. Cell. Neurosci.* 14:578060. doi: 10.3389/fncel.2020.578060

Xu, M., Chen, X., Gu, Y., Peng, T., Yang, D., Chang, R. C., et al. (2013). Baicalin can scavenge peroxynitrite and ameliorate endogenous peroxynitrite-mediated neurotoxicity in cerebral ischemia-reperfusion injury. *J. Ethnopharmacol.* 150, 116–124. doi: 10.1016/j.jep.2013.08.020

Xu, L., Gao, Y., Hu, M., Dong, Y., Xu, J., Zhang, J., et al. (2022). Edaravone dexborneol protects cerebral ischemia reperfusion injury through activating Nrf2/HO-1 signaling pathway in mice. *Fundam. Clin. Pharmacol.* 36, 790–800. doi: 10.1111/fcp.12782

Yang, F., Wang, Z., Zhang, J. H., Tang, J., Liu, X., Tan, L., et al. (2015). Receptor for advanced glycation end-product antagonist reduces blood-brain barrier damage after intracerebral hemorrhage. *Stroke* 46, 1328–1336. doi: 10.1161/STROKEAHA.114.008336

Yepuri, G., Shekhtman, A., Marie Schmidt, A., and Ramasamy, R. (2021). Heme & RAGE: a new opportunistic relationship. *FEBS J.* 288, 3424–3427. doi: 10.1111/febs.15723

Zhang, Y., Sun, J., Zhu, S., Xu, T., Lu, J., Han, H., et al. (2016). The role of rhynchophylline in alleviating early brain injury following subarachnoid hemorrhage in rats. *Brain Res.* 1631, 92–100. doi: 10.1016/j.brainres.2015.11.035

Zhang, L., Wang, H., Cong, Z., Xu, J., Zhu, J., Ji, X., et al. (2014). Wogonoside induces autophagy-related apoptosis in human glioblastoma cells. *Oncol. Rep.* 32, 1179–1187. doi: 10.3892/or.2014.3294

Zhou, X., Wang, X., Li, J., Zhang, M., Yang, Y., Lei, S., et al. (2024). Integrated network pharmacology and in vivo experimental validation approach to explore the potential antioxidant effects of Annao Pingchong decoction in intracerebral hemorrhage rats. *Drug Des. Devel. Ther.* 18, 699–717. doi: 10.2147/DDDT.S439873

Zhu, K., Zhu, X., Liu, S., Yu, J., Wu, S., and Hei, M. (2022). Glycyrrhizin attenuates hypoxic-ischemic brain damage by inhibiting Ferroptosis and Neuroinflammation in neonatal rats via the HMGB1/GPX4 pathway. *Oxidative Med. Cell. Longev.* 2022, 8438528–8438518. doi: 10.1155/2022/8438528

Zou, T., Sugimoto, K., Zhang, J., Liu, Y., Zhang, Y., Liang, H., et al. (2020). Geniposide alleviates oxidative stress of mice with depression-like behaviors by upregulating Six3os1. *Front. Cell Dev. Biol.* 8:553728. doi: 10.3389/fcell.2020.553728